Journal of Materials Chemistry A

PAPER

View Article Online
View Journal | View Issue

Cite this: J. Mater. Chem. A, 2019, 7, 15164

An insight into the effect of azobenzene functionalities studied in UiO-66 frameworks for low energy CO_2 capture and CO_2/N_2 membrane separation†

Nicholaus Prasetya [a] and Bradley P. Ladewig *[ab]

Received 25th February 2019
Accepted 21st May 2019

DOI: 10.1039/c9ta02096a

rsc.li/materials-a

In this paper, a simple approach to study the fundamental aspect of the light-responsive metal–organic framework (MOF) in UiO-66 topology through a mixed-ligand approach is reported. Apart from change in the structural properties, the loading of an azobenzene linker inside the framework also affects the CO_2 light-responsive properties and CO_2/N_2 selectivity which could help to design future low-energy CO_2 adsorbents. Further study to incorporate MOFs into mixed matrix membranes using PIM-1 as the polymer matrix also indicates the benefits of having a higher azobenzene loading in the MOF to enhance the CO_2/N_2 separation performance since it can improve the separation performance that could not be obtained in non-functionalized fillers.

Introduction

During the last decade, metal–organic frameworks (MOF) have gained increased interest. Apart from their exceptionally high surface area and tailorability, one of the interesting properties in the MOF field is the possibility to design them to be responsive towards external stimuli. Such stimuli-responsive MOFs exhibit different behaviours under changing stimuli. Various external stimulants such as pressure,[1] magnetic field,[2] temperature,[3,4] and light[5] can then be used to trigger changes in stimuli-responsive MOFs. Among the stimulants light could be considered as the most convenient to stimulate MOFs because of its abundance.[6] Thus, various research studies have then been conducted in this field and the recent advances have shown its promising applications such as in smart membranes,[7,8] controlled molecular transport,[9] compound release[10–12] and low-energy CO_2 capture.[13] Despite the recent advances in the field, the effect of light-responsive moiety concentration in light-responsive MOFs is still one of the fundamental issues yet to be addressed.[14] This paper then aims to address this challenge by studying this in a UiO-66 type MOF.

Previously, we have reported the successful synthesis of a new and highly robust Azo-UiO-66 MOF.[15] The MOF was synthesized based on UiO-66 synthesis conditions but by replacing the terephthalic acid with 2-phenyldiazenyl terephthalic acid as the ligand. The MOF was found to have a robust structure and exhibit high CO_2/N_2 selectivity and could also experience a highly efficient CO_2 dynamic photoswitching which makes it applicable for post-combustion CO_2 capture. As a quite promising material, Azo-UiO-66 was then further investigated in this study by engineering its structure to obtain a better insight into the effect of the light-responsive moiety inside its framework.

A mixed-ligand approach is one of the promising strategies to accomplish the task. This strategy is quite well-established in the MOF field to control the concentration of a selected ligand inside the MOF, particularly because of its simplicity. The strategy is usually carried out by preparing MOF synthesis solution containing two different ligands at a certain molar ratio. Meanwhile the molar ratio between the metal source and the total ligands in the solution is usually kept the same as that under non-modified synthesis conditions when only one ligand is used. Once the reaction finishes, the resulting products are then expected to have two different linkers inside their framework with different ratios depending on the initial ligand concentration in the solution. This strategy has then been proven successful to synthesize a Dabco-MOF (DMOF) with two different linkers inside its framework.[16] Moreover, this strategy has also been investigated on the UiO-66-NH_2 MOF showing the possibility to control the content of the amino ligand inside the framework by changing the ratio of terephthalic acid and 2-aminoterephthalic acid during the synthesis.[17–19]

Therefore, in this study, the mixed-ligand strategy was employed to control the amount of light-responsive ligand inside the UiO-66 framework. Apart from studying the effect of

[a]Barrer Centre, Department of Chemical Engineering, Imperial College London, Exhibition Road, London, SW7 2AZ, UK

[b]Institute for Micro Process Engineering (IMVT), Karlsruhe Institute of Technology, Hermann-von-Helmholtz-Platz 1, 76344 Eggenstein Leopoldshafen, Germany. E-mail: bradley.ladewig@kit.edu

† Electronic supplementary information (ESI) available. See DOI: 10.1039/c9ta02096a

the light-responsive ligand on MOF properties and its CO_2 capture performance as an adsorbent, this study also aims to investigate its impact once it is incorporated inside a polymer matrix in a mixed matrix membrane form. This is because previous investigations have shown its promising applications for membrane-based CO_2 post-combustion separation. Thus, by combining the study of light-responsive Azo-UiO-66 as a porous adsorbent and as a filler in a mixed matrix membrane, a more comprehensive insight could be expected to understand the effect of having light-responsive ligands inside a MOF.

Experimental section

Synthesis of 2-phenyldiazenyl terephthalic acid (L1)

The modified synthesis of 2-phenyldiazenyl terephthalic acid (L1)[20] used in this study has been previously reported.[15] Briefly, in a typical synthesis, L1 was synthesized by reacting nitrosobenzene and dimethyl aminoterephthalate in glacial acetic acid at 60 °C for 3 days. Afterwards, the glacial acetic acid was evaporated under vacuum and the solution was neutralized using saturated sodium hydrogen carbonate solution. The solution was then extracted using chloroform, dried using $MgSO_4$ and concentrated under vacuum. The product was then purified using column chromatography (hexane : dichloromethane : diethyl ether = 5 : 2.5 : 2.5). The orange product was then concentrated under vacuum to obtain 2-phenyldiazenyl terephthalate.

2-Phenyldiazenyl terephthalate was then dissolved in a mixture of NaOH : methanol : THF overnight. Afterwards, the solution was concentrated under vacuum and 4 M HCl was used to liberate the acid. The acid was back extracted using diethyl ether which was then evaporated under vacuum to obtain L1.

UiO-66 and Azo(*X*)-UiO-66 synthesis conditions

UiO-66 and Azo(*X*)-UiO-66 were synthesized according to a published procedure using acetic acid as the modulator.[15,21] In a typical synthesis, the required amount of $ZrCl_4$ was firstly dissolved in DMF and stirred for 15 minutes. Afterwards, the ligands were added to the solution. For Azo(*X*)-UiO-66, where mixed ligands were used, both L1 and terephthalic acid (L2), the amount of both ligands used in this study is described in detail in Table 1. All the MOFs were then synthesized using a solvothermal method at 120 °C for 24 hours. After cooling down to room temperature, all the products were then collected by centrifugation at 7000 rpm for 6 minutes followed by washing with DMF and methanol, three times each.

CO_2 and CO_2 uptake and CO_2 UV-light responsive test

Prior to measurement, the samples were activated at 110 °C under vacuum overnight. The gas adsorption uptake of CO_2 and N_2 were then measured by using a 3Flex Micromeritics instrument at both 273 and 298 K. Meanwhile, the CO_2 UV-light responsive test was also carried out by using a 3Flex Micromeritics instrument and was based on our previous work.[15] The UV lamp used in the experiment was an Omnicure S1500. During the experiment, the surrounding temperature (both 273 and 298 K) was maintained by using a Micromeritics ISO controller which was filled with a mixture of water and ethylene glycol (50 : 50). For *in situ* measurement using UV-light, various control experiments had also been previously conducted to ensure that the heat generated from the UV light is negligible and does not significantly affect the measurement result.[15,22,23]

Mixed matrix membrane fabrication

The loading of all the mixed matrix membranes (MMMs) was maintained at 10 wt% using PIM-1 as the polymer matrix. PIM-1 was synthesized according to a published procedure.[24] Before membrane fabrication, the MOF was activated at 110 °C. In a typical fabrication, 20 mg of the MOFs and 90 mg of PIM-1 were dispersed in 5 mL dichloromethane to create a homogeneous suspension. The resulting suspension was then stirred overnight. Afterwards, the rest of the PIM-1 was added and the solution was left under stirring overnight. The solution was then cast on a 4 cm Petri dish and covered with perforated aluminum foil to let the solvent evaporate. After the solvent was completely evaporated, the membrane was peeled off from the Petri dish and underwent methanol soaking for 24 hours. This was followed by drying the membrane in an oven at 100 °C overnight to remove all the solvents before gas separation testing. The thickness of the bare polymeric PIM-1 membrane was found to be around 40 μm while the thickness of the mixed matrix membranes was in the range of 60–80 μm.

Membrane gas separation performance study

The complete set-up for the gas separation rig used in this study has been described previously.[23] The membranes were firstly cut into a 2 cm in diameter coupon. These membranes were then mounted onto an aluminum washer and glued the surroundings with epoxy glue to seal the membranes.

The temperature during gas permeation was set at 298 K. Both pure and mixed gas (CO_2 and N_2) were used as the feed gas during the testing. For the mixed gas testing, the ratio of CO_2

Table 1 Synthesis conditions of UiO-66 and Azo(*X*)-UiO-66

MOF	$ZrCl_4$ (mg)	L1 mass (mg) and mol	L2 mass (mg) and mol	L1 : L2 (molar ratio)	DMF (mL)	Acetic acid (mL)
UiO-66	86	0	60 (0.36 mmol)	0	20	0.7
Azo(16.7)-UiO-66	86	25 (0.09 mmol)	45 (0.27 mmol)	1 : 3	20	0.7
Azo(33.3)-UiO-66	86	50 (0.18 mmol)	30 (0.18 mmol)	1 : 1	20	0.7
Azo(66.7)-UiO-66	86	75 (0.27 mmol)	15 (0.09 mmol)	3 : 1	20	0.7
Azo(100)-UiO-66	86	100 (0.36 mmol)	0	—	20	0.7

and N_2 was maintained at 15 : 85 to mimic the power plant flue gas composition. During both pure and mixed gas testing, the feed side pressure was maintained at 20 psia. Meanwhile, the permeate side of the membrane was left at atmospheric pressure with helium gas flowing as the sweep gas. The gas composition was then analyzed using gas chromatography (GC).

Other characterization

Powder X-ray diffraction (PXRD). PXRD diffraction patterns were collected by using a PANalytical instrument. The voltage and current of the instrument during the measurement were set to be 40 kV and 20 mA, respectively. The measurement took place under ambient conditions and the samples were spun. Diffraction patterns were collected between 5 and 40 theta with a 0.008° sample step.

Fourier transform infrared spectroscopy (FTIR). FTIR spectra were collected using an Agilent Cary 630 Spectrophotometer.

Thermogravimetric analysis (TGA). TGA data were collected using a Netzsch TG 209 F1 Libra instrument. About 10 mg of sample was used. The heating rate was set at 5 K per minute under air atmosphere flowing at 20 mL min^{-1}.

UV-vis spectra. UV-vis spectra of the digested MOF were collected using a Thermo Scientific Nanodrop 2000. Approximately, 1 mg sample was used during the experiment and digested in 6% NaOH solution. For the calibration curve, 1 mg of azobenzene ligand was dissolved in 1 mL of NaOH solution to make a stock solution and a series of diluted solutions were made based on the stock solution.

^{1}H-NMR. The ^{1}H-NMR data of the MOF synthesized using the mixed ligand approach were collected using a Bruker NMR instrument equipped with an autosampler. Approximately 2 mg of sample was used and digested in 1 mL of 6% NaOD/D_2O solution.

Scanning electron microscopy (SEM). The micrograph of the gold-sputtered mixed matrix membrane (MMM) cross section was taken using a FEGSEM Sigma 300 instrument. The accelerating voltage was set at 5 kV with the working distance between 10 and 11 mm.

Results and discussion

Azo(*X*)-UiO-66

Synthesis and characterization. The content of the light-responsive ligand in Azo-UiO-66 could be tailored by mixing 2-phenyldiazenyl terephthalic acid (L1) and terephthalic acid (L2) at different molar ratios. This strategy has been previously investigated in UiO-66-NH_2 by mixing L1 and 2-amino-terephthalic acid also at different molar ratios.[17] In this study, 3 different molar ratios of L1 and L2 (25 : 75; 50 : 50 and 75 : 25) were prepared along with UiO-66 (ref. 21) and Azo-UiO-66 (ref. 15) which was synthesized based on a previously reported method. For convenience in this paper, the names of the synthesized UiO-66 frameworks that involved L1 during synthesis are given based on the actual percentage of L1 in the framework after the synthesis (Azo(*X*)-UiO-66, where *X* denotes the percentage of L1 in the actual condition). Therefore, it should be noted that, as will be explained below, the *X* value does not directly correspond to the percentage of the ligand used in the synthesis. Thus, for example, 25% L1 in the synthesis did not give Azo(25)-UiO-66 since the amount of L1 found in the framework was lower.

First, as can be seen in Fig. 1(B), all the synthesis conditions yielded crystalline particles (100–200 nm in size, Fig. S10 in the ESI†) analogous to UiO-66 as proven by the PXRD diffraction patterns showing two characteristic peaks at 7.4° and 8.5° with no additional peaks observed across the observed region. However, it could be seen that the crystallinity of Azo(100)-UiO-66 was found to be the lowest compared with the rest of the MOFs as indicated by low-intensity and broadened peaks. This might have been caused since this MOF only contains bulky L1 in its framework and thus the framework seems to be forced to accommodate the bulky L1 in the framework resulting in reduced crystallinity. This was also previously observed when synthesizing UiO-66 analogue MOFs by using a non-favorable ligand namely *trans*-1,4-cyclohexanedicarboxylate.[25] This reduced crystallinity might then also explain the lower thermal decomposition temperature with a higher azobenzene loading in the UiO-66 framework as observed through TGA analysis (Fig. S8 in the ESI†). However, this does not seem to negatively affect the water stability of the Azo(*X*)-UiO-66 MOFs synthesized using mixed ligand, since the crystallinity of these MOFs could still be maintained after water immersion (Fig. S9 in the ESI†) as also previously observed in UiO-66 [26] and Azo-UiO-66.[15]

Various characterization techniques such as ^{1}H-NMR, UV-vis spectroscopy and ATR-FTIR were then employed to prove and characterize the presence of the mixed-ligand in the resulting MOFs and the complete results are given in the ESI (Fig. S2–S7

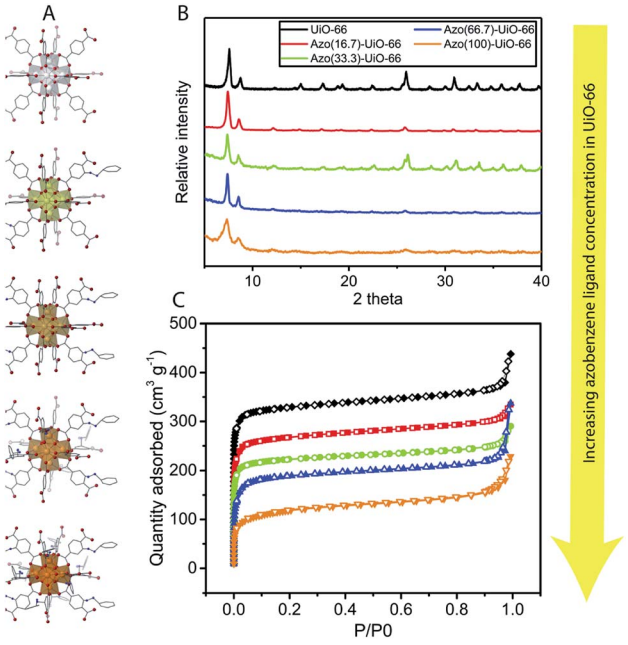

Fig. 1 Hypothetical building unit (A), PXRD diffraction pattern (B) and N_2 adsorption at 77 K (C) of UiO-66 and Azo(*X*)-UiO-66.

in ESI†). As can be seen in Fig. S2–S4 in the ESI,† the digested ^{1}H-NMR spectra of the mixed ligand Azo-UiO-66 show the peaks corresponding to both L1 and L2. The presence of the mixed ligand was also obvious in the UV-vis spectrum of the digested MOFs as presented in Fig. S5 in the ESI.† With a higher concentration of L1 in the synthesis, the absorbance intensity at 322 and 422 nm also increased indicating an increased L1 content in the Azo(*X*)-UiO-66 framework. This is also confirmed by FTIR study showing an increase of relative transmittance at 1370 and 770 cm^{-1} (Fig. S7†) from the azobenzene bonding at a higher azobenzene loading in the framework.[27] This characterization then confirms that both ligands have been successfully incorporated inside the UiO-66 framework.

As a further evaluation, using ^{1}H-NMR, we further calculated the percentage of L1 and L2 in the Azo(*X*)-UiO-66 framework. However, as can be seen in Table S1 in the ESI,† the resulting ligand constituent of Azo(*X*)-UiO-66 frameworks does not correspond to the initial synthesis conditions. This is also corroborated by calculation based on the UV-vis spectrum (Table S2 in the ESI†) as previously suggested.[17] Approximately, it was found that the ratio between L1 and L2 in the Azo(16.7, 33.3 and 66.7)-UiO-66 framework was 2 : 10, 4 : 8 and 8 : 4, respectively. This is different to the previously reported mixed ligand synthesis of UiO-66-NH$_2$ where the ligand constituted in the final framework was in the same ratio as during the initial synthesis.[17] This could be explained by the more bulky structure of L1 compared to L2, which creates a steric hindrance for the metal cluster to coordinate with L1 and thus more favorable to coordinate with L2.

We then studied the effect of azobenzene on the surface properties of the Azo(*X*)-UiO-66 framework. First, it could be seen from Table 2 that the surface area of UiO-66 synthesized in this study was found to be around 1005 m^2 g^{-1} with a maximum pore volume of 0.51 cm^3 g^{-1} which is comparable with other findings.[28] These values then experience gradual reduction as the loading of the azobenzene ligand in the framework was increased, reaching half of the value for Azo(66.7)-UiO-66 and almost 67% reduction for Azo(100)-UiO-66. This then shows that the bulky azobenzene ligand significantly contributes to reducing the available surface in the framework which was also previously observed with incorporating bulky functionalized ligands in the UiO-66 framework.[28,29] Meanwhile, the median pore width of Azo(66.7) and Azo(100)-UiO-66 was found to be higher than of UiO-66, Azo(16.7)-UiO-66 and Azo(33.3)-UiO-66 which was found to be around 0.7 nm. This might be explained by the framework stretching in both MOFs to accommodate more azobenzene in the framework as both of them have the highest azobenzene content inside their framework.

Table 2 Surface area, pore volume and pore width of UiO-66 and Azo(*X*)-UiO-66

MOF	BET surface area (m^2 g^{-1})	Maximum pore volume (cm^3 g^{-1})	Median pore width (nm)
UiO-66	1005	0.51	0.71
Azo(16.7)-UiO-66	821	0.41	0.72
Azo(33.3)-UiO-66	684	0.35	0.70
Azo(66.7)-UiO-66	586	0.29	0.87
Azo(100)-UiO-66	382	0.18	0.91

CO$_2$ adsorption and dynamic photoswitching of Azo(*X*)-UiO-66. Having studied the surface properties of the MOFs, we then studied their application particularly for CO$_2$ capture with the result presented in Fig. 2. Although all Azo(*X*)-UiO-66 MOFs had a lower surface area, we found that only Azo(66.7)-UiO-66 and Azo(100)-UiO-66 experienced lower CO$_2$ adsorption capacity than their UiO-66 parent as can be seen in Fig. 2(A). At 1 bar and 298 K, the CO$_2$ adsorption capacity of both MOFs was found to be around 1 and 0.6 mmol g^{-1} for Azo(66.7)-UiO-66 and Azo(100)-UiO-66, respectively. Meanwhile, the CO$_2$ adsorption capacity of both Azo(16.7) and Azo(33.3)-UiO-66 was not significantly different compared with that of UiO-66 which was around 2.2 mmol g^{-1}. Therefore, to some extent, the presence of protruding azobenzene functionality is beneficial in the UiO-66 framework.

To prove this, the CO$_2$ heat of adsorption (Q_{st}) was calculated. As can be seen in Fig. 2(B), all the Azo(*X*)-UiO-66 MOFs have higher Q_{st} CO$_2$ compared with that of UiO-66 which was around 20–25 kJ mol^{-1} at low coverage and comparable with other findings on UiO-66.[18,29–31] Higher Q_{st} CO$_2$ in the azobenzene-functionalized UiO-66 then indicates the favorable interaction between CO$_2$ and the frameworks containing the azobenzene compound which may arise from Lewis acid–base interaction.[32] However, it could also be seen that an increase in azobenzene concentration does not necessarily lead to an increase in Q_{st} CO$_2$. This is evident from both Azo(66.7)-UiO-66 and Azo(100)-UiO-66 since their Q_{st} CO$_2$ was found to be around 28 kJ mol^{-1} and slightly lower than that of both Azo(16.7)- and Azo(33.3)-UiO-66 which was around 30 and 31 kJ mol^{-1}, respectively. In this case, the steric hindrance imparted by the azobenzene functionality in both Azo(66.7) and Azo(100)-UiO-66 might negatively impact its beneficial aspect as the pore is getting more saturated with azobenzene and thus leaving smaller space for the CO$_2$ adsorption site.

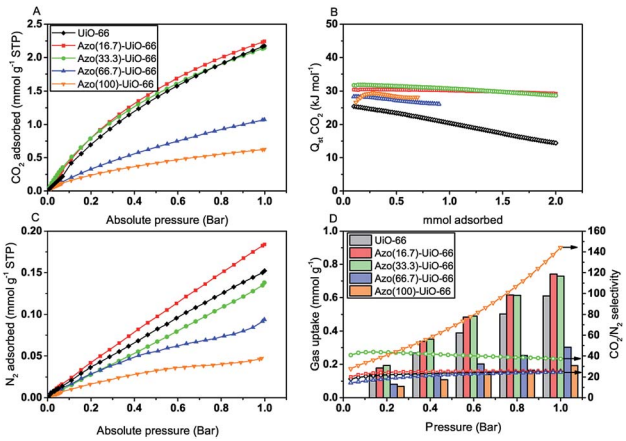

Fig. 2 CO$_2$ adsorption at 298 K (A), Q_{st} CO$_2$ (B), N$_2$ adsorption at 298 K (C) and CO$_2$/N$_2$ IAST selectivity of UiO-66 and Azo(*X*)-UiO-66 (D).

As Azo(*X*)-UiO-66 has favorable interaction with CO_2, it could also be further expected that they could be employed in post-combustion CO_2 capture. We further evaluate this by employing the IAST method as previously described.[33] The result is then presented in Fig. 2(D). From the result, it could be seen that barely any CO_2/N_2 selectivity improvement was observed for both Azo(16.7)- and Azo(66.7)-UiO-66. As can be seen, their value are identical and found to be around 25 which is comparable with the selectivity of non-functionalized UiO-66.[29,34] In contrast, higher selectivity for Azo(33.3)-UiO-66 and an increasing trend for Azo(100)-UiO-66 were observed. Whilst favorable CO_2 interaction could explain the higher selectivity observed in Azo(33.3)-UiO-66, this explanation does not seem fit to explain the increasing trend observed in Azo(100)-UiO-66 as it has slightly lower Q_{st} CO_2 compared with Azo(33.3)-UiO-66. Therefore, favorable CO_2 interaction with the framework alone does not suffice to explain the increased selectivity and another mechanism might play a role in determining the CO_2/N_2 selectivity.

As the azobenzene concentration in the framework increases, it also imparts significant steric hindrance for N_2 adsorption. This is clearly evident in the N_2 adsorption of Azo(100)-UiO-66, as can be seen in Fig. 2(C), where it reached a plateau rather than linearly increasing as pressure increased. As previously observed in azobenzene-containing porous materials, steric hindrance from azobenzene functionality might contribute to a N_2-phobic environment that improves CO_2/N_2 selectivity.[35–37] Therefore, the presence of azobenzene in the Azo-UiO-66 framework does not only enhance the CO_2 interaction with the framework but also contributes to creating a N_2-phobic environment by building a significant steric hindrance inside the MOF. However, this steric hindrance effect cannot be sufficiently built up in Azo(66.7)-UiO-66 as its N_2 uptake was still increasing as opposed to reaching a plateau. As a result, it only suffers from a decrease in CO_2 adsorption capacity while cannot gain a benefit from the steric hindrance imparted by azobenzene resulting in a decrease of CO_2/N_2 selectivity.

Finally, the CO_2 light-responsive properties of Azo(*X*)-UiO-66 were also evaluated based on our previous investigation on Azo-UiO-66 light-responsive properties for low-energy CO_2 capture.[15] The result of this investigation is presented in Fig. 3.

It could be seen from Fig. 3 that all Azo(*X*)-UiO-66 MOFs have lower CO_2 adsorption under UV-light irradiation and the CO_2 could be instantaneously released under dynamic conditions. As previously suggested, the presence of sterically hindered azobenzene inside the UiO-66 framework is believed to contribute to CO_2 release during UV irradiation because of the energy transfer from hindered isomerization to the framework.[38] This phenomenon is different from previously reported azobenzene-based UiO-67 [8] since UiO-67 has a larger pore aperture than UiO-66 which enables it to experience unhindered azobenzene isomerization. The hindered isomerization process is then translated into lower affinity between the MOF and CO_2 upon UV light irradiation as evidenced by Q_{st} CO_2-UV which was found to be around 23–26 kJ mol^{-1} and thus release some of the CO_2 from the framework. In addition, as expected,

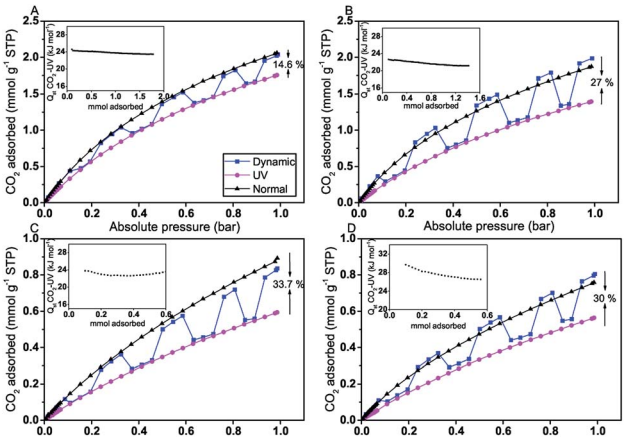

Fig. 3 CO_2 dynamic photoswitching of Azo(16.7) (A), Azo(33.3) (B), Azo(66.7) (C) and Azo(100)-UiO-66 (D) at 298 K. Inset: Q_{st} CO_2 under UV-light irradiation.

higher azobenzene concentration also leads to higher CO_2 desorption capacity. In Azo(16.7)-UiO-66, the UV-induced desorption capacity was found to be around 14%. This value then could be doubled to be about 27% in Azo(33.3)-UiO-66. However, this capacity reached a plateau for both Azo(66.7) and Azo(100)-UiO-66 where only around 30% UV-induced desorption capacity was observed. This could then be explained by the azobenzene configuration inside the framework. Since trans-state azobenzene is more extended and the MOF's pores are fully occupied with the azobenzene ligand, some azobenzene functionalities in Azo(66.7)-UiO-66 and Azo(100)-UiO-66 are likely to be in the *cis*-isomer. As a consequence, they are unable to efficiently absorb the coming UV energy and disperse it to instantaneously release the adsorbed CO_2 resulting in reduction of UV-induced desorption.

Through this CO_2 dynamic photoswitching study combined with the evaluation of the CO_2/N_2 separation ability of Azo(*X*)-UiO-66, a conclusion can then be drawn. Both Azo(16.7)-UiO-66 and Azo(66.7)-UiO-66 are probably not the best candidates from this family. Whilst the former does not have sufficient azobenzene functionalities inside the framework, the latter suffers from standing at the borderline for not having sufficient steric hindrance to provide a N_2-phobic environment that can result in higher CO_2/N_2 selectivity. Meanwhile, although Azo(100)-UiO-66 offers an exceptionally high CO_2/N_2 selectivity, its total uptake and UV-induced desorption capacity are very limited because of the steric hindrance imparted by the azobenzene inside the framework. Thus, Azo(33.3)-UiO-66 could be a better adsorbent candidate for post-combustion CO_2 capture from the Azo(*X*)-UiO-66 family since it shows a good CO_2 uptake capacity while also maintaining a satisfactory level of both CO_2/N_2 selectivity and light-responsive CO_2 desorption capacity to aid its regeneration process.

Azo(*X*)-UiO-66–PIM-1 mixed matrix membranes

Characterization. Having studied the effect of the mixed light-responsive ligand in the UiO-66 framework, we are then

interested in further studying its impact once it is incorporated into a polymer matrix. This is based on our previous studies showing the advantage of having azobenzene functionalities to improve the CO_2/N_2 separation performance in mixed matrix membranes.[15,23] We then chose PIM-1 as the polymer matrix considering its promising performance to surpass the 2008 Robeson upper bound.[39]

All the MMMs were firstly characterized using PXRD, FTIR and SEM. As can be seen in Fig. S14 in the ESI,† all the PXRD diffractograms of the MMMs have the peaks corresponding to the MOFs with two characteristic peaks appearing at 7.4° and 8.5° indicating the presence of UiO-66 and Azo(*X*)-UiO-66 in the structure. Moreover, it could also be observed that the intensity of the PXRD diffractogram is consistent with the PXRD diffractograms of the particles. Higher azobenzene functionality in the MOFs resulted in lower peak intensity and more broadened peaks that might be caused by the less crystalline structure of the MOFs as previously explained. This is particularly evident for Azo(100)-UiO-66–PIM-1.

The presence of the MOF in the PIM-1 matrix was also confirmed through FTIR spectra (Fig. S15 in the ESI†). As can be seen, the FTIR spectra of all MMMs show the peaks that come from both PIM-1 and the MOF. For instance, the characteristic peaks at 1440 and 2239 cm^{-1} could be assigned to C–H bending and CN bonding in PIM-1.[40,41] Once the azobenzene inside the UiO framework was increased, the intensity of peaks at 1390 cm^{-1} and 770 cm^{-1} which is associated with azobenzene bonding also became more evident while these two peaks were not observed in the case of UiO-66–PIM-1 MMMs.

Finally, the presence and distribution of MOFs inside the polymer matrix was also observed through SEM. The cross sectional images of all MMMs are then given in Fig. 4 (additional membrane cross sectional images at lower magnification are also given in Fig. S16–S20 in the ESI†). As can be seen, the structure of all the MMMs is not continuous because of the presence of the MOF and particle agglomerations in all MMMs could also be observed.

Gas separation performance. Having characterized all the MMMs, a CO_2/N_2 gas separation performance test was conducted on the membranes as this is applicable for post-combustion CO_2 separation. First, as can be seen in Fig. 5, the CO_2 permeability of PIM-1 was found to be around 7500 Barrer and comparable with other findings.[42] Regardless of the type of MOF that was incorporated inside the matrix, all the MMMs exhibited higher permeability compared with pristine PIM-1. The permeability could be increased up to 13 000 Barrer in the case of UiO-66–PIM-1, Azo(16.7)-UiO-66–PIM-1 and Azo(33.3)-UiO-66–PIM-1 and around 11 000 Barrer for Azo(66.7)-UiO-66–PIM-1 and Azo(100)-UiO-66–PIM-1. This shows that all the MOFs contribute to adding free volume in the PIM-1 matrix to enhance the gas transport across the membrane. However, it should be noted that Azo(66.7)-UiO-66 and Azo(100)-UiO-66 gave the lowest increase in permeability. This is because both MOFs have the lowest pore volume and CO_2 adsorption capacity compared with the rest of the MOFs resulting in minimal free volume addition in MMMs. This was also corroborated by the CO_2 adsorption measurement conducted on the membrane sample showing a decrease in the total CO_2 uptake for both Azo(66.7)-UiO-66–PIM-1 and Azo(100)-UiO-66–PIM-1 compared with pristine PIM-1.

Although all the membranes gave an identical trend in increasing CO_2 permeability, a difference in CO_2/N_2 selectivity could be observed. First, it could be seen that adding UiO-66 into the PIM-1 matrix only increased the MMM permeability

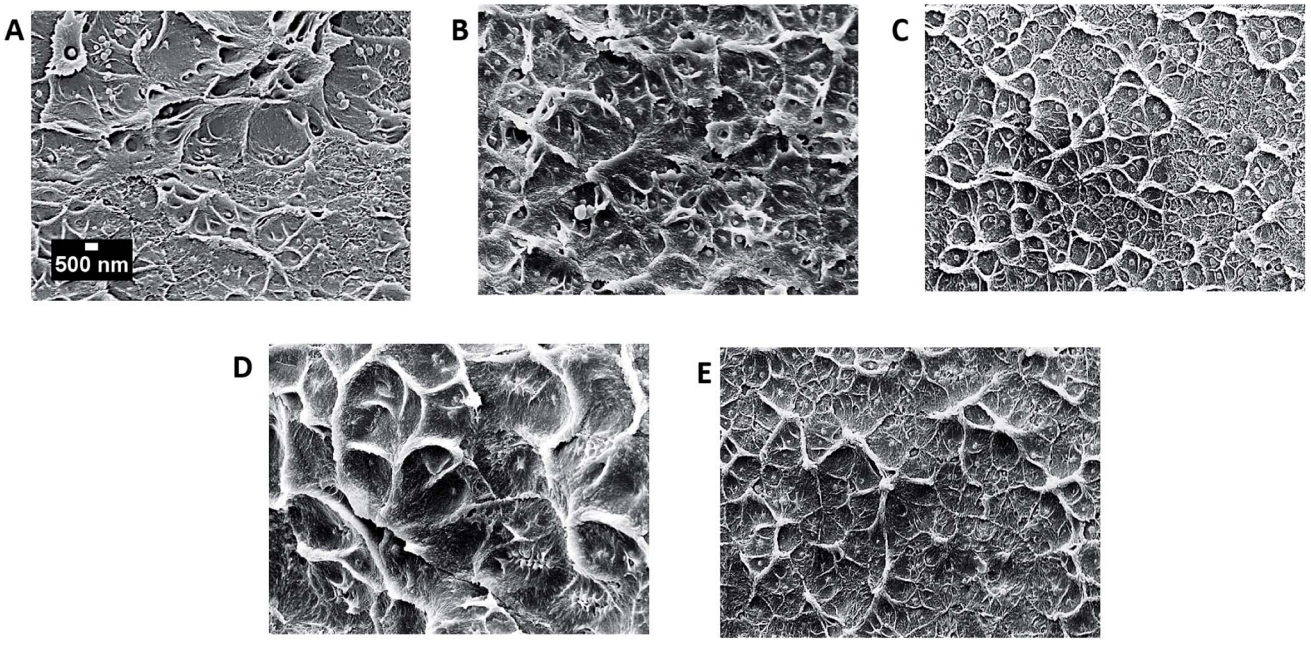

Fig. 4 SEM cross sectional images of PIM-1 MMMs with UiO-66 (A), Azo(16.7)-UiO-66 (B), Azo(33.3)-UiO-66 (C), Azo(66.7)-UiO-66 (D) and Azo(100)-UiO-66 (E) as the fillers.

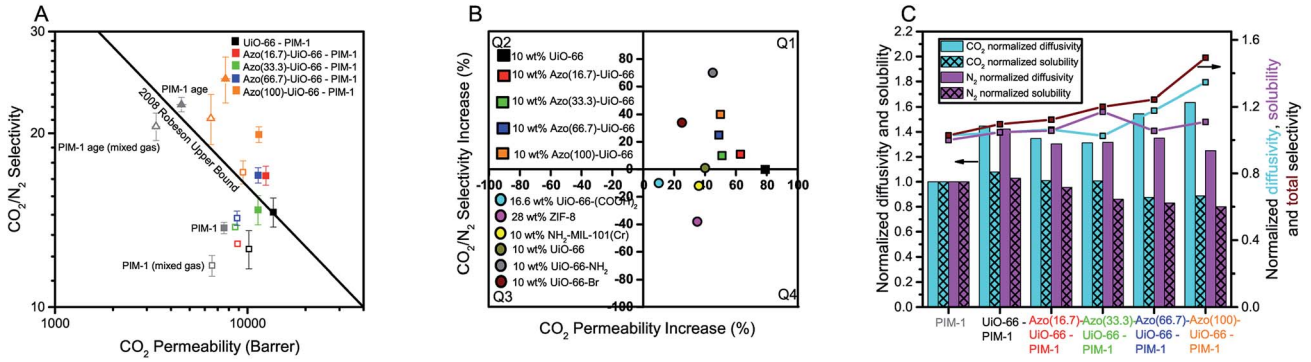

Fig. 5 CO_2/N_2 separation performance of UiO-66–PIM-1 and Azo(*X*)-UiO-66–PIM-1 mixed matrix membranes (square: ideal gas scenario, open square: mixed gas scenario with $CO_2 : N_2 = 15 : 85$, and triangle: aging-mixed gas scenario) (A), their performance improvement compared with MOF-based PIM-1 MMMs[43–46] (B) and the diffusion-solubility calculation of the MMMs (C).

but not the selectivity which was found to be identical at around 14 and comparable with that of pristine PIM-1 in this study and observed elsewhere.[47,48] A different trend started to appear when using the mixed-ligand Azo-UiO-66. The ideal selectivity of pristine PIM-1 could be gradually increased from about 16 in the case of Azo(16.7)-UiO-66–PIM-1 up to around 19 in Azo(100)-UiO-66–PIM-1. This then indicates the importance of having azobenzene functionality in enhancing the MMM performance which was also previously observed with incorporating a nitrogen-rich porous framework in PIM-1 MMMs.[49]

This is also evident when compared with various studies using MOFs as fillers in MMMs as presented in Fig. 5(B). It could be seen that the trend for all the Azo(*X*)-UiO-66–PIM-1 MMMs is to have increasing permeability and selectivity and thus placing them in the middle of Q1. This is an ideal scenario since if defects or non-selective voids exist in the membranes, they will tend to go in the Q4 region where only an increase in permeability is observed without any improvement in selectivity. This ideal situation was also observed in the functionalized UiO-66 family, namely UiO-66-Br and UiO-66-NH_2.[43] This then confirms that the combination of beneficial functional groups for CO_2 capture in UiO-66 with efficient particle dispersion could be utilized to enhance the MMM performance for CO_2/N_2 separation which is hardly obtainable when using non-functionalized fillers such as ZIF-8.[44] Combined with the analysis on the CO_2 permeability values, all the mixed ligand Azo-UiO-66 MMMs could then surpass the 2008 Robeson upper bound separation performance.

As a further evaluation of this positive impact, a mixed feed gas scenario was also studied using a mixture of $CO_2 : N_2$ in a 15 : 85 ratio to simulate the composition of a coal or natural-gas power plant flue gas. As also presented in Fig. 5(A), all the membranes have lower CO_2 permeability compared with their values in pure gas testing which could be explained by the competitive permeation of both gases through the membrane.[49] However, a difference in the selectivity trend was obvious for the MMMs with Azo(*X*)-UiO-66. The mixed gas selectivity of PIM-1 was found to be around 11.4, which is slightly lower compared with its ideal selectivity that was around 14. A similar performance was observed with UiO-66–PIM-1 showing a mixed gas selectivity of around 11.5. For Azo(16.7)-UiO-66, a slight improvement in mixed gas selectivity was observed and it went up to 12.8. As the azobenzene content inside the framework increases, the selectivity value between ideal and mixed gas scenarios starts to get close to each other. Both values were similar in the case of Azo(100)-UiO-66–PIM-1 MMMs and found to be around 19 and 18, respectively.

Therefore, from the results, it could be seen that the ability of Azo-UiO-66 to reject N_2 as observed when it acts as an adsorbent might also be translated to improve the MMM performance during competitive permeation in the mixed-gas scenario. As a further evaluation, diffusivity–solubility coefficients for the membranes were also calculated based on the CO_2 and N_2 adsorption data of the membranes using a scenario of a 15 : 85 $CO_2 : N_2$ mixture based on a previously reported method (Fig. S21 and S22 and detailed calculation is given in Table S3 in the ESI†).[50] The result is then presented in Fig. 5(C). As can be seen, all the MMMs have higher diffusion coefficients compared with pristine PIM-1. This might be explained by the additional free volume contributed by the MOFs to enhance the gas transport across the membrane. Meanwhile, the solubility coefficient seems to be relatively constant or slightly decreased compared with PIM-1 which could be attributed to the lower sorption volume in MMMs compared with pristine membranes.[51]

Despite the similarity in this gas transport properties of all the membranes, a clear difference could be observed regarding the diffusivity and solubility selectivity of the MMMs. It could be seen that both the diffusivity and solubility selectivity of the Azo(*X*)-UiO-66–PIM-1 MMMs show an increasing trend with a higher azobenzene loading inside the framework. Since the solubility coefficient is more related to the thermodynamic properties of a membrane and its affinity towards gases,[51,52] higher solubility selectivity might then be attributed to the lower MMM affinity towards N_2 than CO_2. Although almost all the Azo(*X*)-UiO-66–PIM-1 MMMs showed a lower solubility coefficient towards both gases, the azobenzene functionality inside the MOF does still have favorable interaction with CO_2 as previously indicated through the CO_2 heat of adsorption of the MOFs. As a result, the Azo(*X*)-UiO-66–PIM-1 MMMs have better

affinity towards CO_2 than N_2 resulting in an overall increase in solubility selectivity. Meanwhile, the diffusivity coefficient in gas transport could be related to the physical properties of gases. Two mechanisms may be involved in this case. First, the MOFs might contribute to the rigidification of polymer chains located at the polymer–particle interface. This phenomenon usually results in lower polymer chain mobility in that area and thus increasing diffusivity selectivity.[53] Second, an increase in diffusivity selectivity observed in Azo(*X*)-UiO-66–PIM-1 MMMs could also be explained by the enhancement of the molecular sieving effect inside the MMMs. This is clearly evident as the increasing trend of diffusivity selectivity is more pronounced than solubility selectivity as the azobenzene loading inside the MOF increases. At a higher azobenzene loading inside the framework, more significant steric hindrance could be imparted by the azobenzene functionality in Azo(*X*)-UiO-66 on the MMMs which then contributes to creating a more constrained environment to enhance the molecular sieving properties of the MMMs. Such an enhancement in diffusivity selectivity contributed by the constrained MOF pore environment was also previously observed in fcu-MOF MMMs.[54] Therefore, the selectivity improvement observed in Azo(*X*)-UiO-66–PIM-1 MMMs during the competitive permeation is contributed by more favorably adsorbed CO_2 than N_2, which, once adsorbed, could then be more effectively permeated through molecular sieving enhancement imparted by the azobenzene functionality of the MOFs. A combination of these aspects then contributes to enhancing the overall selectivity of the Azo(*X*)-UiO-66–PIM-1 MMMs.

Finally, as the membrane with the best performance, the aging behavior of Azo-UiO-66–PIM-1 was also evaluated. After 30 days of storage, it could be seen that the MMM still suffered from aging which is characteristic of PIM-1-based membranes.[55,56] This is indicated by the reduction in permeability accompanied by an increase in gas selectivity. In the case of Azo(100)-UiO-66–PIM-1, the permeability dropped to be around 8000 Barrer which is 27% lower than the initial value while the ideal selectivity increased to be around 26 which still put the MMM above the upper bound. This aging rate was also slower than that of pristine PIM-1 which suffered around 40% decline in CO_2 permeability despite its selectivity increase to around 22. Therefore, the presence of Azo(100)-UiO-66 in the PIM-1 matrix might also contribute to improving the aging properties of PIM-1 through polymer chain movement restriction.[55,56] Combined with the improved selectivity of the MMM, this then highlights the importance of azobenzene in the UiO-66 framework and its ability to alter the behavior of PIM-1 for gas separation.

Conclusions

In conclusion, we have shown in this study the effect of azobenzene functionality in UiO-66 type MOFs using a simple mixed ligand approach. The presence of azobenzene functionality not only affects the structural and porosity of the resulting MOFs but can also positively impact their performance as CO_2 adsorbents. Combined with analysis on CO_2 dynamic photoswitching, the MOF with a moderate azobenzene linker loading gave the best performance as a low-energy CO_2 adsorbent candidate. However, the MOF with the highest azobenzene loading was the best option as a filler for MMMs. In this case, the presence of a bulky azobenzene structure is beneficial in decreasing the membrane affinity towards CO_2 which improves the CO_2/N_2 membrane-based separation process.

Data repository

The experimental data and high-resolution images are freely available in the open repository DOI: 10.5281/zenodo.2533852.

Conflicts of interest

There are no conflicts to declare.

Acknowledgements

N. P. acknowledges the PhD scholarship funding from the Department of Chemical Engineering, Imperial College London. The assistance of Mrs Patricia Carry and Mr Kaho Cheung for various analytical techniques is gratefully acknowledged. The assistance of Dr Piers Gaffney, Dr Lorena dos Santos de Souza and Dr Marcus Cook for the ligand synthesis, GC setup and PIM-1 preparation, respectively, is also acknowledged.

References

1 L. Bolinois, T. Kundu, X. Wang, Y. Wang, Z. Hu, K. Koh and D. Zhao, *Chem. Commun.*, 2017, **53**, 8118–8121.
2 H. Li, M. M. Sadiq, K. Suzuki, P. Falcaro, A. J. Hill and M. R. Hill, *Chem. Mater.*, 2017, **29**, 6186–6190.
3 S. Ma, D. Sun, X. Wang and H. Zhou, *Angew. Chem., Int. Ed.*, 2007, **46**, 2458–2462.
4 M. Zhu, X. Song, S. Song, S. Zhao, X. Meng, L. Wu, C. Wang and H. Zhang, *Adv. Sci.*, 2015, **2**, 1500012.
5 H. Li, M. R. Martinez, Z. Perry, H.-C. Zhou, P. Falcaro, C. Doblin, S. Lim, A. Hill, B. Halstead and M. Hill, *Chem.–Eur. J.*, 2016, **22**, 11176–11179.
6 R. Lyndon, K. Konstas, B. P. Ladewig, P. D. Southon, P. C. J. Kepert and M. R. Hill, *Angew. Chem., Int. Ed.*, 2013, **52**, 3695–3698.
7 Z. Wang, A. Knebel, S. Grosjean, D. Wagner, S. Bräse, C. Wöll, J. Caro and L. Heinke, *Nat. Commun.*, 2016, **7**, 13872.
8 A. Knebel, L. Sundermann, A. Mohmeyer, I. Strauß, S. Friebe, P. Behrens and J. Caro, *Chem. Mater.*, 2017, **29**, 3111–3117.
9 K. Müller, J. Helfferich, F. Zhao, R. Verma, A. B. Kanj, V. Meded, D. Bléger, W. Wenzel and L. Heinke, *Adv. Mater.*, 2018, **30**, 1706551.
10 S. Diring, A. Carné-Sánchez, J. Zhang, S. Ikemura, C. Kim, H. Inaba, S. Kitagawa and S. Furukawa, *Chem. Sci.*, 2017, **8**, 2381–2386.
11 M. Nazari, M. RubioâĂŘMartinez, G. Tobias, J. P. Barrio, R. Babarao, F. Nazari, K. Konstas, B. W. Muir, S. F. Collins and A. J. Hill, *Adv. Funct. Mater.*, 2016, **26**, 3244–3249.

12 J. Park, L. Sun, Y. Chen, Z. Perry and H. Zhou, *Angew. Chem.*, 2014, **126**, 5952–5956.
13 N. Prasetya and B. P. Ladewig, *Sci. Rep.*, 2017, **7**, 13355.
14 A. B. Kanj, K. Müller and L. Heinke, *Macromol. Rapid Commun.*, 2018, **39**, 1700239.
15 N. Prasetya, B. C. Donose and B. P. Ladewig, *J. Mater. Chem. A*, 2018, **6**, 16390–16402.
16 L. K. Cadman, J. K. Bristow, N. E. Stubbs, D. Tiana, M. F. Mahon, A. Walsh and A. D. Burrows, *Dalton Trans.*, 2016, **45**, 4316–4326.
17 S. M. Chavan, G. C. Shearer, S. Svelle, U. Olsbye, F. Bonino, J. Ethiraj, K. P. Lillerud and S. Bordiga, *Inorg. Chem.*, 2014, **53**, 9509–9515.
18 J. Ethiraj, E. Albanese, B. Civalleri, J. G. Vitillo, F. Bonino, S. Chavan, G. C. Shearer, K. P. Lillerud and S. Bordiga, *ChemSusChem*, 2014, **7**, 3382–3388.
19 Y. Lee, S. Kim, J. K. Kang and S. M. Cohen, *Chem. Commun.*, 2015, **51**, 5735–5738.
20 J. Park, D. Yuan, K. T. Pham, J.-R. Li, A. Yakovenko and H.-C. Zhou, *J. Am. Chem. Soc.*, 2011, **134**, 99–102.
21 A. Schaate, P. Roy, A. Godt, J. Lippke, F. Waltz, M. Wiebcke and P. Behrens, *Chem.–Eur. J.*, 2011, **17**, 6643–6651.
22 N. Prasetya and B. P. Ladewig, *Sci. Rep.*, 2017, **7**, 41598–42017.
23 N. Prasetya and B. P. Ladewig, *ACS Appl. Mater. Interfaces*, 2018, **10**, 34291–34301.
24 M. Cook, P. R. J. Gaffney, L. G. Peeva and A. G. Livingston, *J. Membr. Sci.*, 2018, **558**, 52–63.
25 B. Bueken, N. Van Velthoven, A. Krajnc, S. Smolders, F. Taulelle, C. Mellot-Draznieks, G. Mali, T. D. Bennett and D. De Vos, *Chem. Mater.*, 2017, **29**, 10478–10486.
26 X. Liu, N. K. Demir, Z. Wu and K. Li, *J. Am. Chem. Soc.*, 2015, **137**, 6999–7002.
27 Q. Yi and G. B. Sukhorukov, *Soft Matter*, 2014, **10**, 1384–1391.
28 S. J. Garibay and S. M. Cohen, *Chem. Commun.*, 2010, **46**, 7700–7702.
29 Z. Hu, M. Khurana, Y. H. Seah, M. Zhang, Z. Guo and D. Zhao, *Chem. Eng. Sci.*, 2015, **124**, 61–69.
30 C. H. Lau, R. Babarao and M. R. Hill, *Chem. Commun.*, 2013, **49**, 3634–3636.
31 Z. Hu, K. Zhang, M. Zhang, Z. Guo, J. Jiang and D. Zhao, *ChemSusChem*, 2014, **7**, 2791–2795.
32 P. Arab, E. Parrish, T. Äřslamoğlu and H. M. El-Kaderi, *J. Mater. Chem. A*, 2015, **3**, 20586–20594.
33 S. Lee, J. H. Lee and J. Kim, *Korean J. Chem. Eng.*, 2018, **35**, 214–221.
34 G. E. Cmarik, M. Kim, S. M. Cohen and K. S. Walton, *Langmuir*, 2012, **28**, 15606–15613.
35 H. A. Patel, S. H. Je, J. Park, D. P. Chen, Y. Jung, C. T. Yavuz and A. Coskun, *Nat. Commun.*, 2013, **4**, 1357.
36 H. A. Patel, S. H. Je, J. Park, Y. Jung, A. Coskun and C. T. Yavuz, *Chem.–Eur. J.*, 2014, **20**, 772–780.
37 S. Zhao, B. Dong, R. Ge, C. Wang, X. Song, W. Ma, Y. Wang, C. Hao, X. Guo and Y. Gao, *RSC Adv.*, 2016, **6**, 38774–38781.
38 S. Castellanos, A. GouletâĂŘHanssens, F. Zhao, A. Dikhtiarenko, A. Pustovarenko, S. Hecht, J. Gascon, F. Kapteijn and D. Bléger, *Chem.–Eur. J.*, 2016, **22**, 746–752.
39 L. M. Robeson, *J. Membr. Sci.*, 2008, **320**, 390–400.
40 Y. Kinoshita, K. Wakimoto, A. H. Gibbons, A. P. Isfahani, H. Kusuda, E. Sivaniah and B. Ghalei, *J. Membr. Sci.*, 2017, **539**, 178–186.
41 L. Hao, K.-S. Liao and T.-S. Chung, *J. Mater. Chem. A*, 2015, **3**, 17273–17281.
42 C. A. Scholes, J. Jin, G. W. Stevens and S. E. Kentish, *J. Polym. Sci., Part B: Polym. Phys.*, 2015, **53**, 719–728.
43 B. Ghalei, K. Sakurai, Y. Kinoshita, K. Wakimoto, A. P. Isfahani, Q. Song, K. Doitomi, S. Furukawa, H. Hirao and H. Kusuda, *Nat. Energy*, 2017, **2**, 17086.
44 A. F. Bushell, M. P. Attfield, C. R. Mason, P. M. Budd, Y. Yampolskii, L. Starannikova, A. Rebrov, F. Bazzarelli, P. Bernardo and J. C. Jansen, *J. Membr. Sci.*, 2013, **427**, 48–62.
45 M. R. Khdhayyer, E. Esposito, A. Fuoco, M. Monteleone, L. Giorno, J. C. Jansen, M. P. Attfield and P. M. Budd, *Sep. Purif. Technol.*, 2017, **173**, 304–313.
46 J. Ma, Y. Ying, X. Guo, H. Huang, D. Liu and C. Zhong, *J. Mater. Chem. A*, 2016, **4**, 7281–7288.
47 C. L. Staiger, S. J. Pas, A. J. Hill and C. J. Cornelius, *Chem. Mater.*, 2008, **20**, 2606–2608.
48 J. Ahn, W.-J. Chung, I. Pinnau, J. Song, N. Du, G. P. Robertson and M. D. Guiver, *J. Membr. Sci.*, 2010, **346**, 280–287.
49 X. Wu, Z. Tian, S. Wang, D. Peng, L. Yang, Y. Wu, Q. Xin, H. Wu and Z. Jiang, *J. Membr. Sci.*, 2017, **528**, 273–283.
50 A. Sabetghadam, X. Liu, M. Benzaqui, E. Gkaniatsou, A. Orsi, M. M. Lozinska, C. Sicard, T. Johnson, N. Steunou and P. A. Wright, *Chem.–Eur. J.*, 2018, **24**, 7949–7956.
51 J. Ahn, W.-J. Chung, I. Pinnau and M. D. Guiver, *J. Membr. Sci.*, 2008, **314**, 123–133.
52 F. Moghadam, M. R. Omidkhah, E. Vasheghani-Farahani, M. Z. Pedram and F. Dorosti, *Sep. Purif. Technol.*, 2011, **77**, 128–136.
53 T.-S. Chung, L. Y. Jiang, Y. Li and S. Kulprathipanja, *Prog. Polym. Sci.*, 2007, **32**, 483–507.
54 G. Liu, V. Chernikova, Y. Liu, K. Zhang, Y. Belmabkhout, O. Shekhah, C. Zhang, S. Yi, M. Eddaoudi and W. J. Koros, *Nat. Mater.*, 2018, **17**, 283.
55 S. J. D. Smith, C. H. Lau, J. I. Mardel, M. Kitchin, K. Konstas, B. P. Ladewig and M. R. Hill, *J. Mater. Chem. A*, 2016, **4**, 10627–10634.
56 C. H. Lau, P. T. Nguyen, M. R. Hill, A. W. Thornton, K. Konstas, C. M. Doherty, R. J. Mulder, L. Bourgeois, A. C. Y. Liu and D. J. Sprouster, *Angew. Chem., Int. Ed.*, 2014, **53**, 5322–5326.